

Experimental Investigation on the Effect of a Microsecond Pulse and a Nanosecond Pulse on NO Removal Using a Pulsed DBD with Catalytic Materials

V. R. Chirumamilla¹ · W. F. L. M. Hoeben¹ · F. J. C. M. Beckers¹ ·
T. Huiskamp¹ · E. J. M. Van Heesch¹ · A. J. M. Pemen¹

Received: 21 August 2015 / Accepted: 1 October 2015 / Published online: 20 October 2015
© Springer Science+Business Media New York 2015

Abstract In this study, an experimental investigation of the removal of NO from an atmospheric air stream has been carried out with a non-thermal plasma dielectric barrier discharge reactor filled with different catalytic materials. TiO₂, CuO–MnO₂–TiO₂, CuO–MnO₂–Al₂O₃ catalysts were used to study the synergy between the plasma and the catalysts. The NO_x removal efficiency and by-products formation were studied as a function of energy density, pulse rise time and width using a plasma catalytic configuration. It was observed that the shorter pulses are more efficient for NO_x removal but at the expense of higher by-products formation such as N₂O and O₃. A comparison has been made between an in-plasma catalytic configuration and a post-plasma catalytic configuration. Among all the three catalysts that were studied, CuO–MnO₂–TiO₂ catalyst showed the best performance with respect to the removal efficiency as well as the by-products formation in both the in-plasma and the post-plasma catalytic configuration. In general, the post-plasma configuration showed better results with respect to low by-products formation.

Keywords Non-thermal plasma · Dielectric barrier discharge · N₂O · O₃ · NO conversion

Introduction

One of the main sources of air pollution is the transportation sector. Motor vehicles emissions include unburned hydrocarbons (UHCs), carbon monoxide (CO), carbon dioxide (CO₂), nitrogen oxides (NO_x), sulfur oxides (SO_x) and particulate matter (PM). According to the European Environment Agency 2009 data (EEA-32), the transportation sector contributes around 58, 21, 27 and 22 % of NO_x, SO_x, PM_{2.5} and PM₁₀ emissions

✉ V. R. Chirumamilla
v.r.chirumamilla@tue.nl

¹ Department of Electrical Engineering, Eindhoven University of Technology, P.O. Box 513, 5600 MB Eindhoven, The Netherlands

respectively [1]. These emissions are significant as they have a negative impact on human health. With increasing concerns about these impacts, the introduction of emission control standards has been started. According to Euro6 standards for passenger cars, the emission limits for petrol NO_x , Diesel NO_x and Diesel PM are 60, 80 and 5 mg/km respectively [2]. With increasingly stringent regulations, the lower limits of the emissions standards could be reached by efficient reduction of UHCs, NO_x , SO_x , and PMs coming from the exhaust.

Non-thermal plasma appears to be a promising technology for decomposition of gaseous pollutants with relatively low energy consumption [3–5]. The high energy electrons produced in non-thermal plasma by the electrical discharge collide with the gas molecules to generate radicals such as reactive oxygen species (OH , HO_2 , H_2O_2 , O^3P , ^1D , ^1S), $\text{O}_2[\text{a}^1\Delta_g]$, O_3), metastables (N^4S , ^2D , ^2P), $\text{N}_2[\text{A}^3\Sigma_u^+$, B , $\text{a}^1]$), and ions (O_4^+ , O_4^- , O_5^- , O_2^- , O^- , and so on) by electron-impact dissociation and ionization. The mentioned reactive oxygen species induce oxidative degradation of the pollutants.

Non-thermal plasma is able to oxidize NO to NO_2 [6–9] which is further converted to HNO_3 and HNO_2 in the presence of water vapor. Without the help of a catalyst, NO_x cannot be reduced to N_2 just with electrical discharges. From literature, it is clear that using a catalyst with a plasma reactor can enhance the product selectivity and the energy efficiency [10]. Yamamoto et al. [11] concluded that the operating cost of a plasma-chemical hybrid system is approximately 15 times more economical compared to the conventional selective catalytic reduction process. Hence, plasma-assisted catalysis is a promising way for improved pollutant removal efficiency and selectivity. Also, the production of unwanted by-products can be minimized.

Non-thermal plasma can be generated at atmospheric pressure and at ambient temperature with various techniques such as with glow discharges, corona discharges, pulsed discharges, dielectric barrier discharges (DBDs), microwave and radio frequency discharges [12, 13]. DBDs are widely used for VOCs and NO_x reduction. There have been various arrangements proposed in the literature to combine a plasma reactor with a catalytic reactor such as a one-stage configuration, or in-plasma catalytic configuration (IPC), and a two-stage configuration, or post-plasma catalytic configuration (PPC) [14–16]. In both of these configurations, different catalysts have been tested and are reported in literature. $\gamma\text{-Al}_2\text{O}_3$ [17, 18], TiO_2 [19], Al_2O_3 loaded with different metals such as Ag [20], Pd [19], and In [21], TiO_2 loaded with BaTiO_3 [22] and $\text{V}_2\text{O}_5\text{-WO}_3$ [23] and zeolites [24] are among the various catalysts that have been tested with non-thermal plasma. An overview of the published papers on NO_x removal is presented in Table 1. Combining a plasma reactor with a catalytic reactor can help in reducing the NO and NO_2 to molecular nitrogen with minimum by-products if the plasma operating conditions are selected carefully [18].

The two main approaches that were reported in literature to improve the energy efficiency of the DBD plasma reactor was the development of the discharge mode and coupling the plasma with catalysts. The first approach includes optimizing the reactor configuration and the power source. The major parameters of the power source that should be tuned to improve the efficiency of the plasma are the frequency, voltage, and the waveform of the voltage. In this present study, the pulse waveform of the voltage has been studied and pulse parameters such as pulse repetition rate, pulse rise time and pulse width are varied as they play an important role in changing the reaction chemistry. Puchkarev et al. stated in their study on energy-efficient plasma processing of gaseous emission that the efficiency of NO_x reduction is a complex function of parameters that includes pulse width, pulse polarity, current density, repetition rate, and reactor design. Careful

Table 1 Literature on NO removal with plasma-catalysis

| Reactor configuration | Conditions | Catalyst | Conversion | Energy density | Application | Refs. |
|----------------------------|-------------------------------------------------------------------------------------------------------------------------------------------|--------------------------------------------------------------------|----------------------------------|--------------------|--------------------|-------|
| DBD | T: 773 K | Indium doped: Al ₂ O ₃ | Approx. 60 % @ 473 K | 700 J/L | Diesel engines | [21] |
| | V: 3–16 kV Addition of primary alcohols Initial NO conc: 1000 ppm V: 5 kV with 50 Hz power input GHSV: 14,400 h ⁻¹ | | > 90 % @ 623 K > 80 % @ 773 K | 100 J/L 100 J/L | | |
| Cylindrical DBD | | Ag/USY Ag/Al ₂ O ₃ | | | | [28] |
| SDBD | Wet gas Initial NO conc: 100 ppm 60 Hz AC power supply | γ-Al ₂ O ₃ | Approx 60 % | 133 J/L | Automobiles | [17] |
| Packed DBD | Initial NO conc: 200 ppm Initial NO conc: 300–500 ppm | BaTiO ₃ | Approx 96 % | 55.5 J/L | Flue gas emissions | [18] |
| Packed DBD (pulsed corona) | NO ₂ : 15–50 ppm Frequency: 300–350 pulses/sec Addition of methanol as additive (1000 ppm) T: 150 °C | γ-Al ₂ O ₃ | Approx 66 % | 140 J/L | Exhaust gases | [22] |
| | | BaTiO ₃ + γ-Al ₂ O ₃ (1:5 ratio) | 60 % | 140 J/L | | |
| Packed DBD | Initial NO conc: 570 ppm Frequency: 900 Hz pulse/sec @ 9 kV Gas flow rate: 5 L/min T: 298 K | γ-Al ₂ O ₃ + TiO ₂ (1:1 ratio) | 21 % | 140 J/L | Exhaust gases | [29] |
| | | Co-ZSM-5 post-plasma | 78 % | 60 J/L | | |
| | | TiO ₂ coated glass beads Degussa P-25 PCVD method | 80 % 58 % | | | |

Table 1 continued

| Reactor configuration | Conditions | Catalyst | Conversion | Energy density | Application | Refs. |
|-----------------------|---------------------------------------------------------------------------------------------------|--------------------------------------------------------------------------------------------------------------------------------------------------|--------------------------------------------------------------------------------------------------------|-----------------------------|----------------------|-------|
| DBD | Initial NO conc: 500 ppm NH ₃ : 500 ppm Gas flow rate: 25 L/min T: 100–250 °C | V ₂ O ₅ –WO ₃ /TiO ₂ Ethene as additive | 55 % @ 100 °C 70 % @ 100 °C | 80 J/L | Diesel exhaust gases | [23] |
| DBD | Initial NO conc: 500 ppm Propene: 0–2000 ppm Gas flow rate: 1 L/min | Al ₂ O ₃ TiO ₂ ZrO ₂ Alumosilicate Pd/Al ₂ O ₃ Ag/mordenite | 60 % @ 300 °C 15 % @ 350 °C 55 % @ 300 °C 20 % @ 300 °C 10 % @ 230 °C 30 % @ 325 °C | | Diesel exhaust gases | [19] |
| Cylindrical DBD | T: 250 °C Initial NO conc: 400 ppm | Cu–ZSM-5 | Approx. 40 % @ 273 K Approx. 25 % @ 473 K | 3.5 W 3.5 W | Flue gas | [30] |
| Coaxial-type DBD | Initial NO conc: 360 ppm T: 110 °C | γ-Fe ₂ O ₃ | Approx. 44 % | 50 J/L | | [31] |
| DBD | Initial NO conc: 1200 ppm | Ag/Al ₂ O ₃ | > 50 % @ 250 °C > 74 % @ 250 °C > 90 % @ 350 °C | 60 J/L 180 J/L 60 J/L | Marine engines | [20] |

optimization of all these parameters is required to reach cost effective NO_x reduction [25]. In [25], the authors also mentioned that the short-duration pulses are more effective than the longer pulses with respect to the energy cost. It was observed that the energy utilization will be more efficient with respect to remediation if the given amount of energy is deposited with a high repetition rate of short duration pulses [26]. The second approach was to combine plasma with appropriate catalysts [27], which will also be done in the present study.

In this study, a pulsed non-thermal DBD reactor at atmospheric pressure is combined with catalysts such as TiO₂, CuO–MnO₂–TiO₂, CuO–MnO₂–Al₂O₃ to study the synergy between the plasma and the catalysts in terms of removal efficiency and energy efficiency. Also, the effect of pulse parameters was studied by using a microsecond pulse source and a nanosecond pulse source. A microsecond pulse with 0.9-μs rise time and 2-μs pulse width (referred to as μs pulse in this paper) and a nanosecond pulse with 10-ns rise time and 16-ns pulse width (referred to as ns pulse in this paper) were used. The effect of catalyst, energy density, and the pulse rise time on the NO removal efficiency and the energy efficiency is reported. A comparison has been made between the two different plasma-catalytic configurations: IPC and post-plasma configuration.

The first part of the paper describes the experimental setup including the reactor, the catalytic materials and the power sources that have been used. Details of NO conversion and by-products formation as a function of rise time with the plasma alone reactor and with plasma-catalytic reactor are given in the second part. An overview of the comparison of IPC and PPC using the microsecond and the nanosecond pulses with respect to energy density and by-products formation at 90 % conversion of NO is also presented in the second part.

Experimental Setup

The entire experimental setup can be explained in four main parts. The DBD reactor, the gas feeding system, the electrical part (pulse source and electrical measurements) and the gas diagnostics as shown in Fig. 1.

DBD Reactor

A schematic representation of the DBD-plasma reactor setup is shown in Fig. 2. The plasma reactor is made of quartz with a diameter of approximately 14 mm and with a thickness of 2 mm. The reactor consists of two electrodes, a high-voltage electrode and a grounded electrode. The high-voltage electrode that is connected to the high-voltage power source is made up of a stainless-steel rod with a diameter of 1.5 mm and is mounted at the centre of the reactor. The steel mesh around the reactor acts as the grounded electrode. The IPC and the PPC configurations of this DBD reactor used in the experiments are shown in Fig. 3.

Catalysts

The three different catalysts that were used in this study were TiO₂, CuO–MnO₂–TiO₂, CuO–MnO₂–Al₂O₃ and were supplied by Heraeus, Hanau, Germany. The characteristics of the catalysts are presented in Table 2. The TiO₂ pellets were in anatase form and was

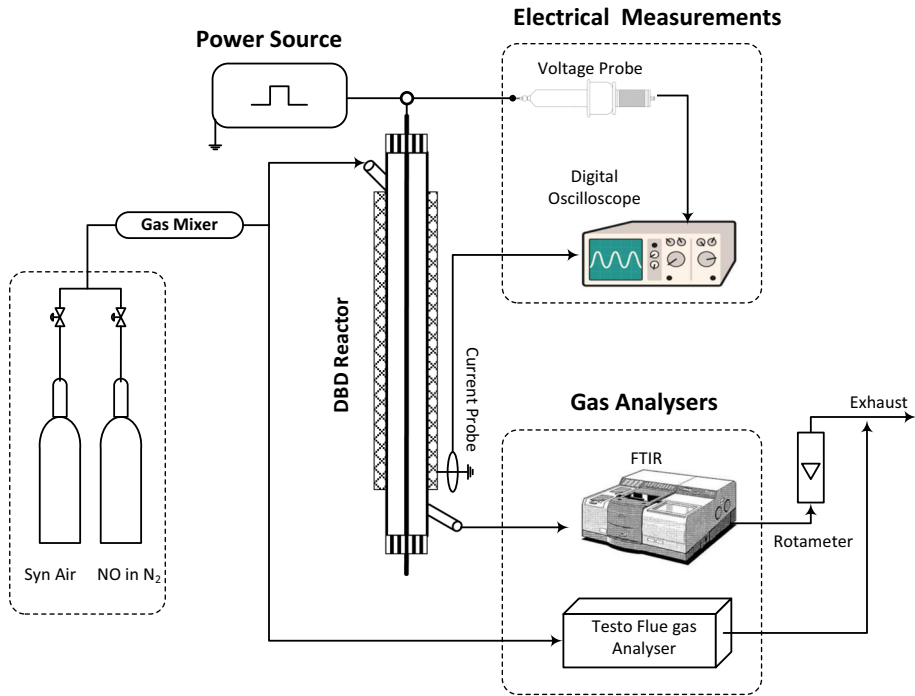


Fig. 1 Schematic overview of the experimental setup with pulsed DBD reactor for NO removal

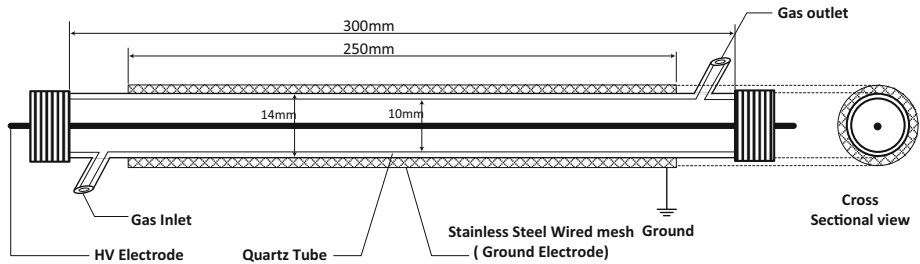


Fig. 2 Cross-sectional view of the cylindrical quartz tube DBD reactor operating at ambient temperature and atmospheric pressure

chosen because of its photocatalytic nature. Numerous authors have studied the ozone decomposition potential of MnO₂ in the plasma-catalytic configurations for VOC's reduction [32–37]. It will be interesting to study the effect of loading material on the performance of NO conversion and by-products formation by comparing the results of TiO₂ catalyst with CuO–MnO₂–TiO₂ catalyst. Morales et al. [38] in their study on Mn–Cu mixed oxide catalysts for ethanol oxidation, found out that the presence of copper improves the catalytic performance in ethanol total oxidation and they also found out that MnCu/TiO₂ 673 and MnCu/ZrO₂ 873 catalysts are the most active and selective to CO₂ [39]. It will be interesting to look at the effect of support by comparing the results of CuO–MnO₂–TiO₂ catalyst with CuO–MnO₂–Al₂O₃ catalyst.

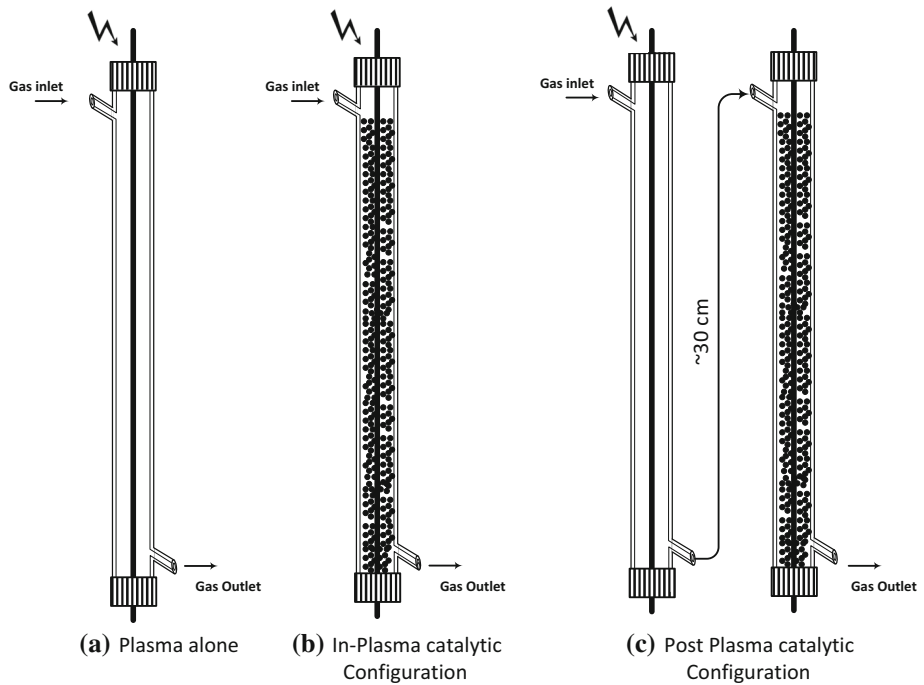


Fig. 3 Schematic overview of the plasma alone configuration and the two plasma-catalytic configurations that are used in the experiments of this paper. (Note in (c), the catalytic reactor is not powered)

Table 2 Heraeus specifications of the catalysts that are used in the experiments of this paper

| Catalyst | Shape | Size (mm) | BET surface area (m ² /g) | Bulk density (Kg/m ³) | Composition |
|------------------------------------------------------|-------------|-----------|--------------------------------------|-----------------------------------|-------------------------------------|
| TiO ₂ | Cylindrical | 1.5 | 50 | 925 | 75 % anatase |
| CuO–MnO ₂ –TiO ₂ | Cylindrical | 1.5 | 50 | 925 | 3 wt% CuO, 6.8 wt% MnO ₂ |
| CuO–MnO ₂ –Al ₂ O ₃ | Spherical | 2 | 80 | 800 | 30 wt% Cu–mn-oxide |

Gas Concentration Measurements

The gas used in the experiments discussed in this paper consists of a mixture of NO in N₂ (10,000 ppm of NO in N₂ base) and synthetic air. Synthetic air (<3 ppm H₂O content) is used to dilute NO to get the desired initial concentration. The initial concentration of nitrogen oxide used in this study is 200 ppm as it will be easy to compare the results with the available literature. The gas mixture is dosed at room temperature and atmospheric pressure. The composition of the gas is tested with a Testo 350 XL flue gas analyser and the flow was controlled by mass flow controllers. The treated gas from the DBD reactor was sampled out to a Fourier Transform Infrared Spectrometer (FTIR, BRUKER Tensor

27) with a 20-cm optical path gas cell to measure the exit gas concentration. The resulting spectra from the FTIR are used to calculate the varying concentrations of NO, NO₂, O₃ and N₂O. With these concentrations, the removal efficiency of the DBD reactor could be calculated. The conversion of NO is determined with:

$$\text{NO conversion} = \frac{[\text{NO}]_i - [\text{NO}]_o}{[\text{NO}]_i} \times 100, \quad (1)$$

where [NO]_i and [NO]_o are the inlet concentration of NO to the reactor and the outlet concentration of NO from the reactor respectively.

For the quantitative measurements of by-products, the FTIR was calibrated for N₂O and O₃. N₂O calibration was done by using 10,000 ppm of N₂O in N₂ calibration gas and the O₃ calibration was done by UV-absorption spectrometry.

Power Source

Microsecond (μs) Pulse Source

The schematic representation of the MOSFET-based solid state microsecond pulse power source is shown in Fig. 4. The buffer capacitor C₁ of the circuit is charged to 25 V via a transformer and rectifier. Capacitor C₂ will be charged to approximately 300 V during operation. When MOSFET M₁ is closed, C₂ is discharged via the high-voltage pulse transformer T₂ generating a 17-kV pulse on the secondary side. M₁ remains still closed after the pulse and the current through L₁ will linearly increase via C₁–L₁–D₁–L_{pri}–M₁ and thus energy is stored in L₁. When MOSFET M₁ is opened, the current through L₁ free-wheels into C₂ charging the capacitor to 300 V again and the magnetization current of the transformer is able to freewheel via the R₁–D₂ snubber circuit. The stray inductance and parasitic capacitance of the high-voltage winding limit the rise time of the pulse. The typical rise time of the pulse is 0.9 μs and the pulse width is 2 μs. The maximum repetition rate (f) of the source is 1000 pulses/second.

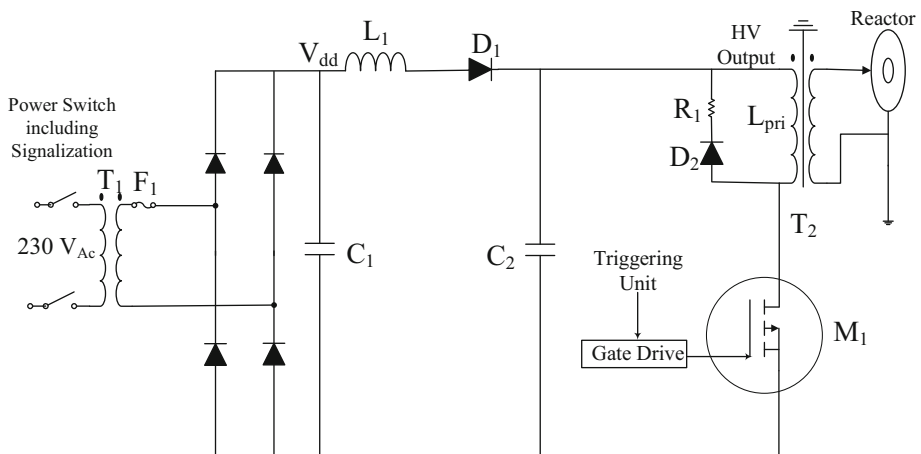


Fig. 4 Schematic overview of the MOSFET based solid state microsecond pulse power source

Nanosecond (ns) Pulse Source

The schematic of the spark-gap based high-voltage nanosecond pulse circuit is shown in Fig. 5. Pulse generation is realized by first charging capacitor C_1 in <10 ms by a 60-kV DC power supply. Resistor R_1 limits the charging current and prevents a near short circuit of the power supply output when the spark gap fires. The spark gap consists of three disc-shaped electrodes (two gaps). A trigger unit applies a 30-kV pulse (μ s rise-time) to the center electrode which causes the right gap to fire. The current path of the trigger discharge is via D_1 – R_2 – SG – R_3 . The full voltage on C_1 will now be over the left and center electrode causing the full spark-gap to fire. Capacitor C_1 will be rapidly discharged (in <100 ns) into the 50Ω coaxial cable, creating the high-voltage pulse on the output of the cable. R_2 is added to protect the trigger unit from transient voltages and possible voltage reversal on C_1 . Energy transferral to the reactor stops after the plasma in the reactor quenches, usually due to the dropped output voltage of the source. The spark gap remains closed until all energy in the circuit is consumed. Resistor R_3 dissipates all residual energy in the circuit, including reflections due to improper impedance matching between the reactor and the coaxial cable. Resistor R_3 has a high impedance during the initial pulse generation ($R_3 \gg Z_{cable}$) and consumes only a small amount of energy during that time. The maximum repetition rate of the source is 100 pulses/second.

Electrical Measurements

The typically applied voltage and discharge current for both the microsecond pulse and the nanosecond source are shown in the Figs. 6 and 7 respectively. A Northstar PVM-5 high-voltage probe and a Pearson 6600 current probe were used to measure the voltage over the reactor and the discharge current respectively. These two probes were connected to a Lecroy Wavesurfer 454 oscilloscope to measure the electrical power consumption. The voltage amplitude was kept constant (17-kV for the μ s pulse source and 40-kV for the ns pulse source) and the pulse repetition rate was varied to vary the energy density. The pulse repetition rate of the μ s pulse source can be varied from 1 Hz–1 kHz whereas the ns pulse source between 1–100 Hz. The energy per pulse [E_p , (J)] is calculated by using Eq. (2).

$$E_p = \int_{pulse} V(t)I(t)dt \tag{2}$$

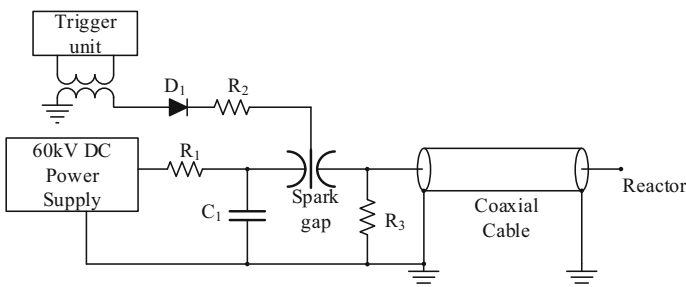


Fig. 5 Schematic overview of the spark-gap based high-voltage nanosecond pulse circuit

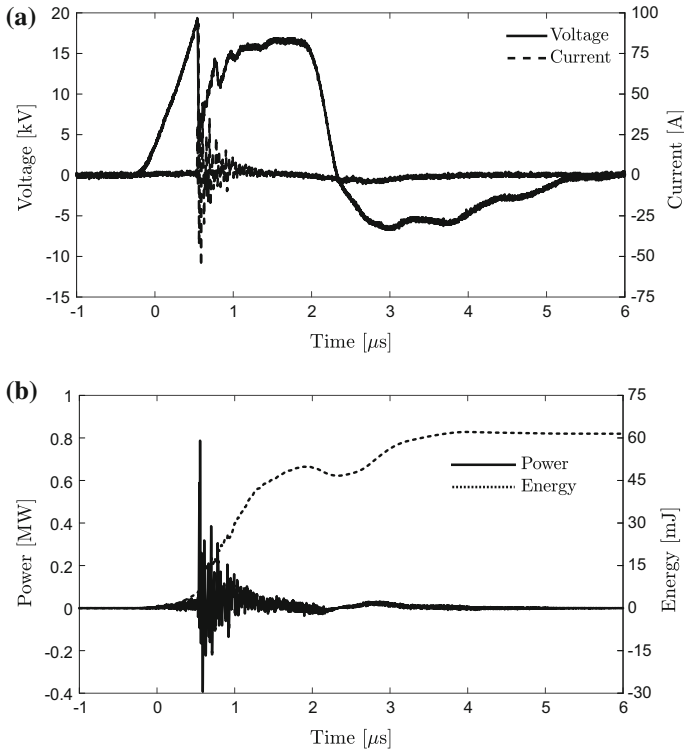


Fig. 6 Typical waveforms in the DBD reactor with the μs pulse source **a** applied voltage and discharge current **b** power and energy deposited per pulse

$V(t)$ and $I(t)$ in Eq. (2) represent the measured voltage and current respectively. The energy measurements were taken after the voltage and current reach a stable end value. The calculated power and energy per pulse are also given in Figs. 6 and 7 respectively.

It can be observed that in the nanosecond voltage and current waveform, oscillations occur. These oscillations and reflections might occur due to mismatch between the output impedance of the power source and the reactor impedance. The energy density [ε , (J/L)] was used as a parameter to compare the efficiency of treatments with different plasma-catalytic configurations and with different rise times. The energy density is defined as the energy deposited into the gas per unit volume and can be calculated by using Eq. (3). F in Eq. (3) is the volumetric gas flow through the reactor (L/s)

$$\varepsilon = \frac{fE_p}{F} \tag{3}$$

The energy yield represented by W-value in eV/NO molecule and the removal efficiency of NO represented by G-value in mol/J are obtained by using Eqs. (4) and (5) respectively.

$$W\text{-value} = \frac{V_m \times \varepsilon}{\Delta[\text{NO}] \times 10^{-6} \times N_a \times e} \quad (\text{eV/NO molecule}) \tag{4}$$

$$G\text{-value} = \frac{\Delta[\text{NO}] \times 10^{-6}}{V_m \times \varepsilon} \quad (\text{mol/J}) \tag{5}$$

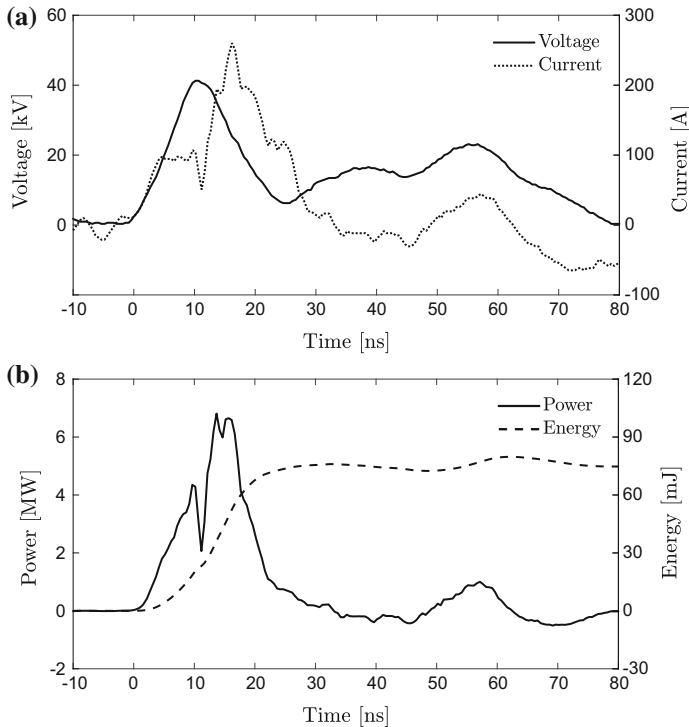


Fig. 7 Typical waveforms in the DBD reactor with the ns pulse source **a** applied voltage and discharge current **b** power and energy deposited per pulse

where $\Delta[\text{NO}]$ is the amount of NO removed in ppm. V_m is the molar volume which is 24.48 L/mol at 20 °C and 1 atm. N_a is the Avagadro number and e is the charge of the electron.

Results and Discussion

The experiments were carried out with a plasma-alone reactor configuration as shown in Fig. 3a and plasma combined with the following catalysts: TiO_2 , $\text{CuO-MnO}_2\text{-TiO}_2$, $\text{CuO-MnO}_2\text{-Al}_2\text{O}_3$ (Fig. 3b, c). The voltage was kept constant (17-kV for the μs pulse source and 40-kV for the ns pulse source) and the pulse repetition rate was used as the operating parameter to vary the energy densities.

Plasma Alone Configuration

NO Conversion as a Function of Pulse Rise Time

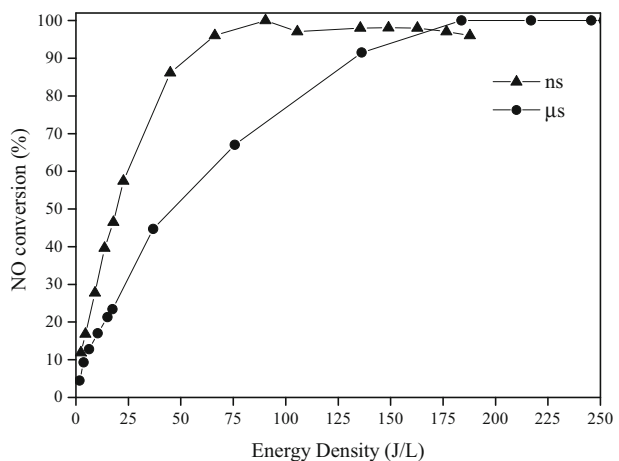
A μs pulse with a rise time of 0.9 μs and width of 2 μs and a ns pulse source with a rise time of 10 ns and width of 16 ns were used to study the effect of the pulse parameters on the NO conversion and the by-products formation. The voltage was kept constant (17-kV for the μs pulse source and 40-kV for the ns pulse source) and the pulse repetition rate was varied to

vary the energy density. Figure 8 shows the effect of pulse parameters on the NO conversion. It was observed that the ns pulse reaches 100 % NO conversion at low energy densities compared to the μ s pulse. An energy density of approximately 60 and 130 J/L were required for 100 % NO conversion using the ns and the μ s pulse respectively. This 100 % conversion of NO by the ns pulse at low energy densities is due to the ability of the short rise times to produce high E/N (electric field/number density) [40]. The W-value was 90 and 184 eV/NO molecule respectively for the ns pulse and the μ s pulse at 25 J/L as seen in Fig. 9. The results of Fig. 9 also show that with increasing energy density, the W-value increases and keeps increasing even after 100 % NO removal. The increase in the W-value even after 100 % NO conversion is due to the fact that there is no NO left for further conversion and the energy input to the reactor is used in the other reactions such as production of O_3 , N_2O and other unwanted by-products formation. The input energy is also dissipated in the form of light and heat. Figure 9 also shows that there is a decrease in the G-value with increasing energy density. This is simply because the G-value is inversely proportional to the W-value.

Effect of the Pulse Rise Time on the By-Products Formation

The effect of the energy density on the by-products formation such as O_3 and N_2O are studied with respect to the rise time as shown in Fig. 10. It can be noticed that both the ns pulse and the μ s pulse produce by-products. The production of by-products is more pronounced with the ns pulse rise time compared to the μ s pulse. It is observed that for 100 % NO conversion, approximately 6 and 14 ppm of N_2O and O_3 , respectively, are generated for the ns pulse. Whereas for the μ s pulse, N_2O and O_3 formation is 3 and 2 ppm respectively. The ns pulse is efficient in converting 100 % NO at low energy densities but at the expense of higher by-products formation. At higher energy densities, collisions between the electrons and the neutrals are more frequent which leads to the production of more O and N atoms as shown in Eqs. (6) and (7). Thus the produced O and N atoms react with O_2 and NO_2 to produce O_3 and N_2O respectively as shown in the Eqs. (8)–(10) and can be seen in Fig. 10 with a steep rise in O_3 concentration. As noticed in the Fig. 11, the NO_2 concentration exhibits a maximum for both ns pulse and μ s pulse. It can also be noted

Fig. 8 NO conversion as a function of the energy density with the nanosecond pulse source and the microsecond pulse source



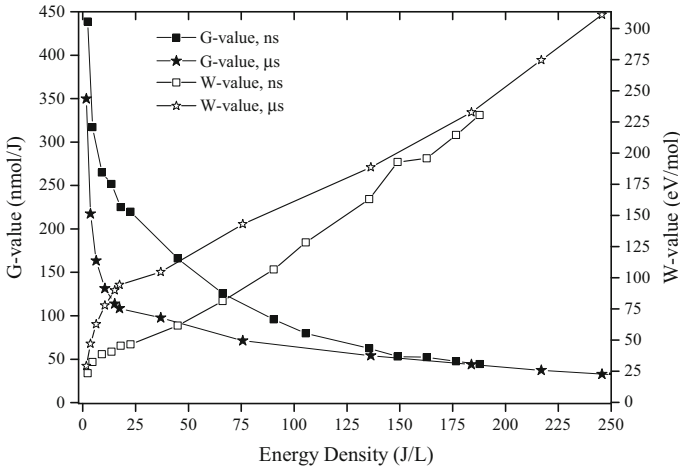


Fig. 9 W-value as a function of energy density with the nanosecond pulse source and the microsecond pulse source

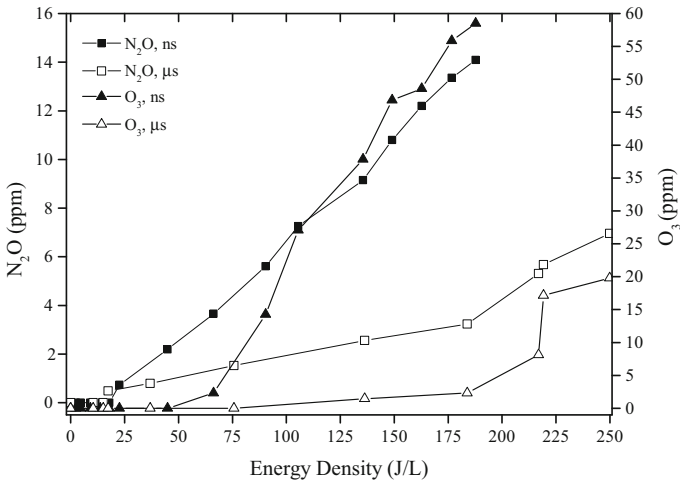


Fig. 10 N₂O and O₃ formation as a function of the energy density with the nanosecond pulse source and the microsecond pulse source

that at higher energy densities (above 80 J/L for the ns pulse), the produced O atoms react with NO₂ to regenerate a small amount of NO (Eq. 11) which is why a 100 % NO conversion is not achieved for high energy densities as seen in Fig. 8.



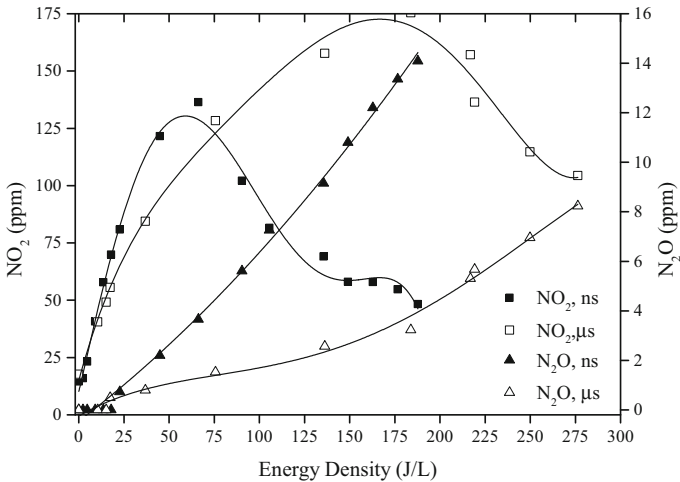


Fig. 11 NO_2 and N_2O formation as a function of energy density with the nanosecond pulse source and the microsecond pulse source



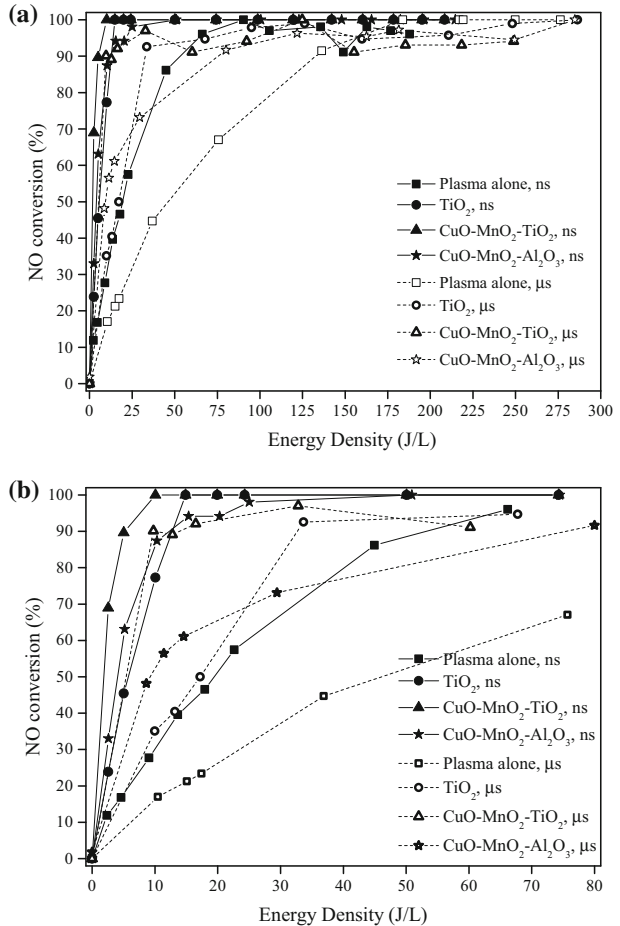
Plasma-Assisted Catalysis

In this section, the effect of the catalysts combined with the plasma as a function of the energy density and the pulse rise time were investigated. Both the IPC and the PPC configurations were studied. The arrangements of these configurations is as shown in Fig. 3b, c.

Enhancement Effect of Plasma and Catalyst with In-Plasma Catalytic Configuration

A pulsed DBD is combined with catalysts such as TiO_2 , $\text{CuO-MnO}_2\text{-TiO}_2$ and $\text{CuO-MnO}_2\text{-Al}_2\text{O}_3$ to study the synergy between the plasma and the catalysts in terms of the NO removal efficiency and the energy efficiency. The NO conversion as a function of the energy density for the plasma-alone configuration and the IPC is shown in Fig. 12. The figure shows that, $\text{CuO-MnO}_2\text{-TiO}_2$ catalyst is capable of removing 100 % NO at low energy densities compared to $\text{CuO-MnO}_2\text{-Al}_2\text{O}_3$ and TiO_2 . The ns pulse shows better removal efficiency with both the plasma alone configuration and the IPC. But, as mentioned earlier, higher NO conversion at lower energy densities is at the expense of higher by-products formation. Figures 13 and 14 show the production of N_2O and O_3 respectively as a function of the energy density. It is obvious that the plasma-alone configuration produces more N_2O compared to the IPC. The ns pulse produces higher amounts of N_2O and O_3 in both the plasma alone and with the IPC. The trend is slightly different for TiO_2 and $\text{CuO-MnO}_2\text{-Al}_2\text{O}_3$ as these catalysts produced higher amounts of N_2O and O_3 with

Fig. 12 NO conversion as a function of energy density for various catalysts with in-plasma catalytic configuration with the nanosecond pulse source and the microsecond pulse source. **a** Overview. **b** Detailed view



the μ s pulse for 100 % NO conversion compared with the ns pulse. It is also observed that TiO₂ produced higher amounts of O₃ compared to the plasma alone configuration, CuO–MnO₂–TiO₂, CuO–MnO₂–Al₂O₃ catalysts. This increased amount of O₃ generation may be due to the production of electron-hole pairs by TiO₂ when exposed to a mean energy greater than 3.2 eV [15]. The electrons produced by the TiO₂ surface converts oxygen molecules into oxygen anion radicals(O₂⁻) which further reacts with the holes on the surface of TiO₂ producing more oxygen atoms. This oxygen anion further reacts with oxygen molecules to produce ozone as shown in Eqs. (12)–(17). Thus, TiO₂ tends to follow more oxidative pathway and produces more ozone. The increase in ozone generation was also observed in the study [41] where the authors investigated ozone production in a surface dielectric barrier discharge reactor with a TiO₂ catalyst.



Fig. 13 N_2O formation as a function of energy density for various catalysts with in-plasma catalytic configuration with the nanosecond pulse source and the microsecond pulse source

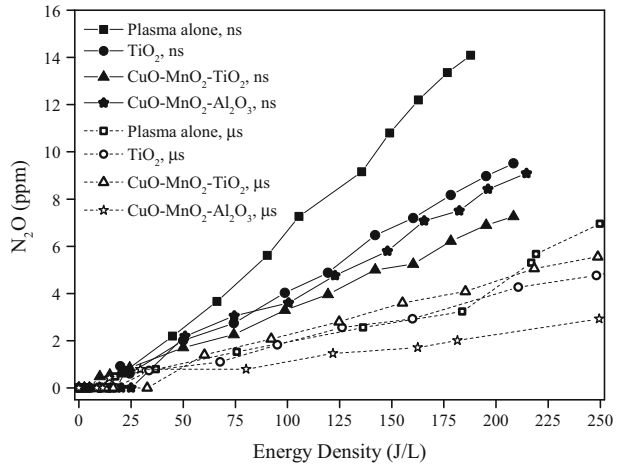
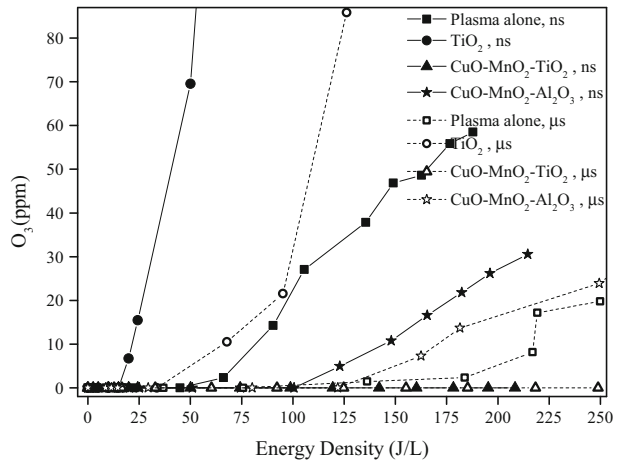


Fig. 14 O_3 formation as a function of energy density for various catalysts with in-plasma catalytic configuration with the nanosecond pulse source and the microsecond pulse source



MnO_x -based catalysts showed better performance with respect to ozone decomposition. This may be due to the insitu decomposition of ozone into atomic oxygen on the surface where this atomic oxygen will be present on the MnO_x surface in the form of $O(^3P)$. This in turn might oxidizes NO to NO_2 which might be the possible reason for the better performance of the MnO_x -based catalysts with respect to ozone decomposition. As mentioned in [37], the better performance of $CuO-MnO_2-TiO_2$ can be attributed to the synergy

between the plasma excitation and the photocatalytic behaviour of TiO_2 . Even though MnO_x -based catalysts proved to be efficient in ozone decomposition, it is also observed from the results of this study that $\text{CuO-MnO}_2\text{-Al}_2\text{O}_3$, at higher densities failed to decompose ozone. This may be due to the difference in the support materials. With a change in the dielectric constant of the support material, there could be a change in the plasma distribution or plasma discharges or in the adsorption-desorption effects of the molecules. The effect of catalyst support was studied in [42] where the authors investigated the effect of the catalyst support in the degradation of the odorous compounds by the plasma and found out that there were differences in the electric behaviour and the space development of plasma with different supports.

Enhancement Effect of Plasma and Catalyst with Post-Plasma Catalytic Configuration

For the PPC configuration, two identical reactors were connected in series as shown in Fig. 3c. The gas input is to the reactor where the electrode is connected to the power supply. The output gas from this reactor is sent to the reactor filled with catalytic material. The effect of the energy density on the removal efficiency for the PPC is shown in Fig. 15. It is observed that, $\text{CuO-MnO}_2\text{-TiO}_2$ catalyst is capable of removing 100 % NO at low energy densities with both the μs and the ns pulses compared with $\text{CuO-MnO}_2\text{-Al}_2\text{O}_3$ and TiO_2 . Thus, the $\text{CuO-MnO}_2\text{-TiO}_2$ catalyst showed better performance with both the IPC and the PPC. Also, the shorter pulses showed better performance with both the IPC and the PPC with respect to the removal efficiency. It can be seen from Fig. 16 that the ns pulse resulted in higher amounts of N_2O formation with the PPC as well. There is a clear distinction between the μs and ns pulses with respect to N_2O formation. TiO_2 showed higher amounts of N_2O formation with the IPC compared to the PPC with both the μs and the ns pulses where as $\text{CuO-MnO}_2\text{-Al}_2\text{O}_3$ showed higher N_2O formation with the PPC with the ns pulse only. In general, the PPC performed better with both the μs and the ns pulse with respect to the ozone destruction irrespective of the catalysts used as shown in Fig. 17.

With the IPC, TiO_2 generated high amounts of ozone where as with the PPC, no ozone formation was detected. This can be explained by the fact that, in the IPC, the electrons in the discharge having a mean energy of 3–4 eV can activate TiO_2 either by electron-impact or by photon absorption or by both. However, in the PPC this mechanism is not possible as the photons and electrons produced by the plasma discharges cannot enter the catalytic reactor; only the long lived reactive species and intermediates can. Ozone from the plasma reactor entering the catalytic reactor, might get adsorbed on the active site and gets decomposed into oxygen and an active O radical. This active O radical combines with ozone to form oxygen and excited oxygen. This excited oxygen decomposes into oxygen leaving the active site of the catalyst. The reaction pathways or the plausible mechanisms of O_3 decomposition on the catalytic surface are mentioned in [32, 43].

Figures 18 to 20 show an overview of the comparison of the IPC and the PPC using the μs and the ns pulses with respect to the energy density and the by-products formation at 90 % conversion of NO. Among all the three catalysts that were studied, $\text{CuO-MnO}_2\text{-TiO}_2$ catalyst showed better performance with respect to NO conversion as well as by-products formation with both the IPC and the PPC. The IPC with the TiO_2 catalyst produced higher levels of O_3 , especially with the μs pulse. This high production of O_3 with

Fig. 15 Removal efficiency as a function of energy density for various catalysts with post-plasma catalytic configuration with the nanosecond pulse source and the microsecond pulse source. **a** Overview. **b** Detailed view

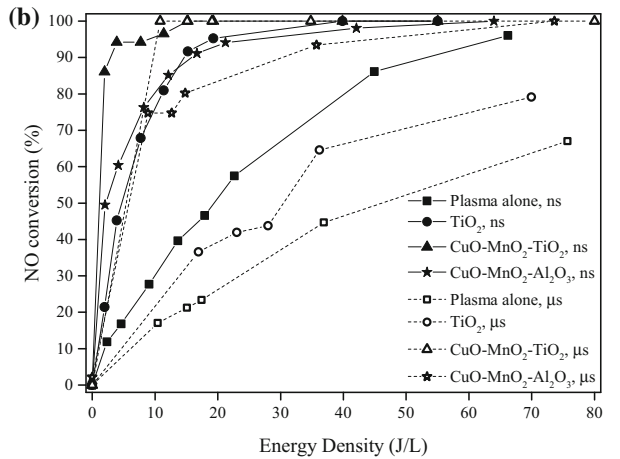
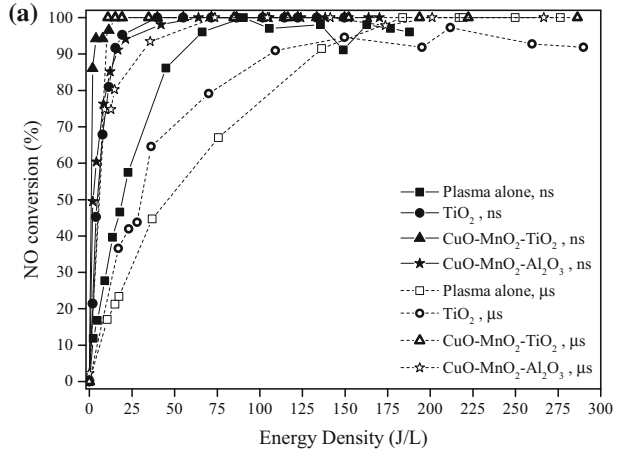


Fig. 16 N₂O formation as a function of energy density for various catalysts with post-plasma catalytic configuration with the nanosecond pulse source and the microsecond pulse source

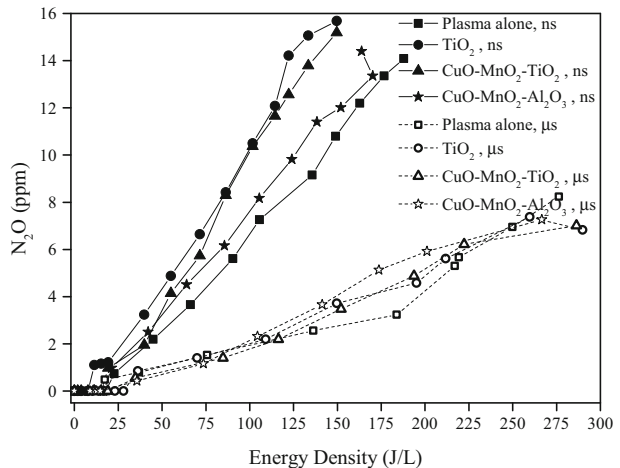


Fig. 17 O₃ formation as a function of energy density for various catalysts with post-plasma catalytic configuration with the nanosecond pulse source and the microsecond pulse source

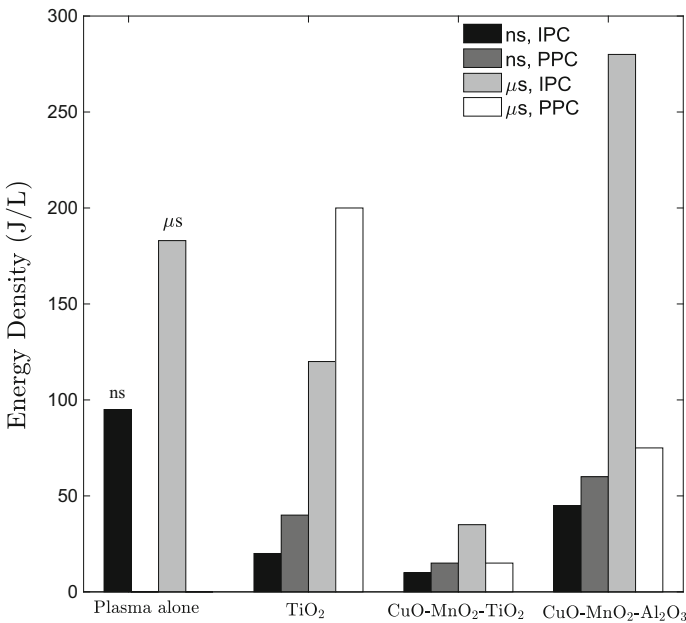
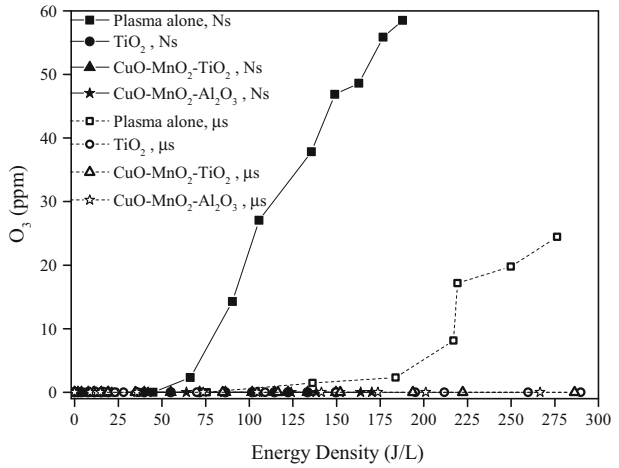


Fig. 18 Overview of the energy density at 90 % NO conversion with plasma alone configuration and plasma-catalytic configuration with the nanosecond pulse source and the microsecond pulse source

the μs pulse is due to the fact that the 90 % conversion of NO was obtained at higher energy densities for the μs pulse than the ns pulse. In general, the PPC showed better results with respect to both the NO removal and the by-products formation except for N₂O formation with TiO₂ and CuO–MnO₂–Al₂O₃ catalysts.

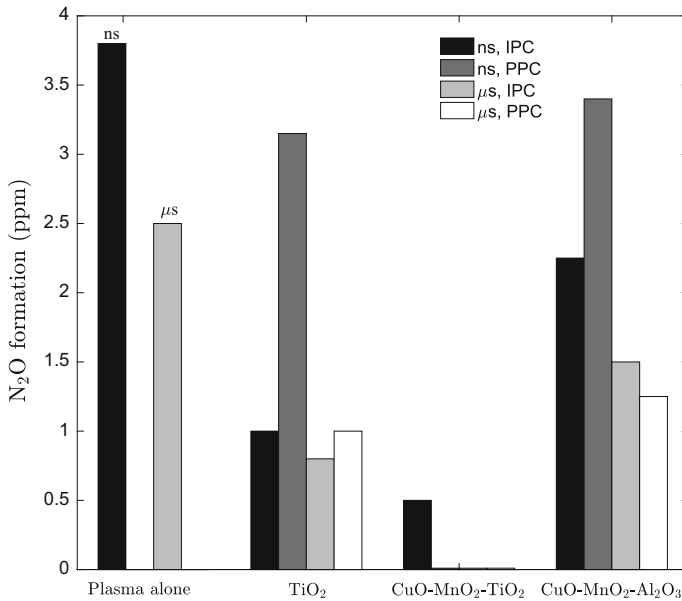


Fig. 19 Overview of N₂O formation at 90 % NO conversion with plasma alone configuration and plasma-catalytic configuration with the nanosecond pulse source and the microsecond pulse source

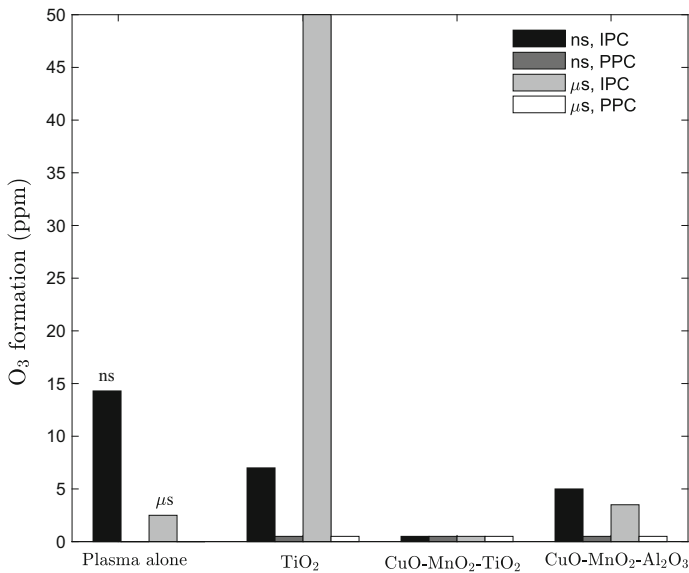


Fig. 20 Overview of O₃ formation at 90 % NO conversion with plasma alone configuration and plasma-catalytic configuration with the nanosecond pulse source and the microsecond pulse source

Table 3 Comparison between different plasma-catalytic configurations on NO removal and by-products formation with the nanosecond pulse source and the microsecond pulse source at 90 % NO conversion

| Plasma condition | Energy density (J/L) | O ₃ production (ppm) | N ₂ O production (ppm) |
|--------------------------------------------------------------------|----------------------|---------------------------------|-----------------------------------|
| Plasma (ns) | + | – | – |
| IPC with TiO ₂ (ns) | ++ | + | + |
| IPC with CuO–MnO ₂ –TiO ₂ (ns) | ++ | ++ | ++ |
| IPC with CuO–MnO ₂ –Al ₂ O ₃ (ns) | + | + | – |
| Plasma (μs) | o | – | – |
| IPC with TiO ₂ (μs) | o | – | o |
| IPC with CuO–MnO ₂ –TiO ₂ (μs) | ++ | ++ | ++ |
| IPC with CuO–MnO ₂ –Al ₂ O ₃ (μs) | – | + | – |
| PPC with TiO ₂ (ns) | ++ | ++ | – |
| PPC with CuO–MnO ₂ –TiO ₂ (ns) | ++ | ++ | ++ |
| PPC with CuO–MnO ₂ –Al ₂ O ₃ (ns) | + | ++ | – |
| PPC with TiO ₂ (μs) | – | ++ | o |
| PPC with CuO–MnO ₂ –TiO ₂ (μs) | ++ | ++ | ++ |
| PPC with CuO–MnO ₂ –Al ₂ O ₃ (μs) | + | ++ | o |

Conclusions

In this study, an experimental investigation on the removal of NO from an atmospheric air stream has been carried out with a NTP dielectric barrier discharge reactor. The DBD is combined with catalysts such as TiO₂, CuO–MnO₂–TiO₂, CuO–MnO₂–Al₂O₃ to study the synergy between the plasma and the catalysts in terms of the NO conversion and the energy efficiency. Also, the effect of the pulse parameters was studied by varying the pulse repetition rate, the pulse rise time and the pulse duration. A μs pulse with a rise time of 0.9 μs and width of 2 μs and a ns pulse source with a rise time of 10 ns and width of 16 ns were used to study the effect of pulse parameters on the NO conversion and the by-products formation. The effect of the catalyst, energy density and the pulse rise time on the NO conversion and the energy efficiency were reported. A comparison has been made between different plasma-catalytic configurations such as an IPC and a PPC as shown in Table 3. Where the symbols in Table 3 ++, +, o and – indicates that the specific configuration showed the best performance, good performance, satisfactory performance and unsatisfactory performance respectively.

It was observed that the ns pulse is more efficient for NO conversion but at the expense of higher by-products formation. An energy density of 95 and 183 J/L was required for 100 % NO conversion using the ns and the μs pulse respectively. For 100 % NO conversion, the generated N₂O and O₃ was approximately 6 and 14 ppm respectively for the ns pulse whereas it was 3 and 2 ppm of N₂O and O₃ respectively for the μs pulse. CuO–MnO₂–TiO₂ catalyst showed better performance with respect to the NO conversion as well as the by-products formation with both the IPC and the PPC. It was also observed that TiO₂ produced higher amounts of O₃ with the IPC but on the other hand with the PPC, TiO₂ yielded no ozone. In general, the PPC showed better results with respect to by-products formation. Table 4. presents a quick comparison of where the current study stands with respect to that obtained from the published results. It is very difficult to get a common

Table 4 Comparison of NO conversion efficiency of the reactor configurations used in the current study with that of others present in the literature

| Reactor configuration | Conditions | Catalyst | Energy density | Conversion |
|------------------------------------|----------------------------------------------------------------------------------------------------------------------------------------------------------|------------------------------------------------------------------------------------------------------------------------------------------------------------------------------------------------------------------------------------------------------------------|----------------------------------------------------------|-----------------------------------------------------------------------|
| DBD [21] | T: 773 K V: 3–16 kV Addition of primary alcohols Wet gas | Indium doped: Al ₂ O ₃ | 700 J/L 100 J/L 100 J/L 133 J/L | Approx. 60 % @ 473 K >90 % @ 623 K >80 % @ 773 K Approx 60 % |
| SDBD [17] | Initial NO conc: 100 ppm 60 Hz AC power supply | γ -Al ₂ O ₃ | 55.5 J/L | Approx 96 % |
| Packed DBD [18] | Initial NO conc: 200 ppm | BaTiO ₃ | | |
| Packed DBD (pulsed corona) [22] | Initial NO conc: 300–500 ppm NO ₂ : 15–50 ppm Frequency: 300–350 pulses/sec Addition of methanol as additive (1000 ppm) T: 150 °C | γ -Al ₂ O ₃ BaTiO ₃ + γ -Al ₂ O ₃ (1:5 ratio) γ -Al ₂ O ₃ + TiO ₂ (1:1 ratio) Co-ZSM-5 post-plasma | 140 J/L 140 J/L 140 J/L 60 J/L | Approx 66 % 60 % 21 % 78 % |
| DBD [23] | Initial NO conc: 500 ppm NH ₃ : 500 ppm Gas flow rate: 25 L/min T: 100–250 °C | V ₂ O ₅ -WO ₃ /TiO ₂ Ethene as additive | 80 J/L | 55 % @ 100 °C 70 % @ 100 °C |
| Coaxial-type DBD [31] | Initial NO conc: 360 ppm T: 110 °C | γ -Fe ₂ O ₃ | 50 J/L | Approx. 44 % |
| DBD [20] | Initial NO conc: 1200 ppm | Ag/Al ₂ O ₃ | 60 J/L 180 J/L 60 J/L | >50 % @ 250 °C >74 % @ 250 °C >90 % @ 350 °C |
| DBD [Present work] | Initial NO conc: 200 ppm Gas flow rate: 2 L/min Frequency: 1–100 pulses/sec Pulse rise time: 10 ns | TiO ₂ IPC TiO ₂ PPC CuO-MnO ₂ -TiO ₂ IPC CuO-MnO ₂ -TiO ₂ PPC CuO-MnO ₂ -Al ₂ O ₃ IPC CuO-MnO ₂ -Al ₂ O ₃ PPC | 10 J/L 10 J/L 10 J/L 10 J/L 10 J/L 10 J/L | 77 % 78 % 98 % 95 % 87 % 78 % |

platform for comparison as the parametric variations form a wide spectrum. Within a limited set of variations, the results have been presented and it can be inferred that the present reactor configurations have yielded a better conversion efficiency at room temperature itself. However, detailed experimental investigations at higher flow rates and with real diesel exhaust are presently being carried out which will be the scope of future paper.

References

1. European environment agency. <http://www.eea.europa.eu/data-and-maps/indicators/transport-emissions-of-air-pollutants-8/transport-emissions-of-air-pollutants-9>. Accessed 12 April 2014
2. European automobile manufacturers association. <http://www.acea.be/industry-topics/tag/category/euro-standards>. Accessed 12 April 2014
3. Hammer T, Kappes T, Baldauf M (2004) Plasma catalytic hybrid processes: gas discharge initiation and plasma activation of catalytic processes. *Catal Today* 89(1):5–14
4. Oda T, Kato T, Takahashi T, Shimizu K (1997) Nitric oxide decomposition in air by using non-thermal plasma processing-with additives and catalyst. *J Electrostat* 42(1):151–157
5. Chang JS (2001) Recent development of plasma pollution control technology: a critical review. *Sci Technol Adv Mater* 2(3):571–576
6. Penetrante B, Hsiao M, Merritt B, Vogtlin G, Wan C (1997) Plasma-assisted heterogeneous catalysis for NO_x reduction in lean-burn engine exhaust. technical report, DTIC Document
7. Penetrante BM, Brusasco RM, Merritt BT, Vogtlin GE (1999) Environmental applications of low-temperature plasmas. *Pure Appl Chem* 71(10):1829–1835
8. Sun M, Ravi V (2010) Role of oxygen in the plasma catalytic removal of NO_x. *VIVECHAN IJR* 1(2):1–9
9. Beckers FJCM, Hoeben WFLM, Pemen aJM, van Heesch EJM (2013) Low-level NO_x removal in ambient air by pulsed corona technology. *J Phys D Appl Phys* 46:295201
10. Neyts E, Bogaerts A (2014) Understanding plasma catalysis through modelling and simulation a review. *J Phys D Appl Phys* 47(22):224010
11. Yamamoto T, Okubo M, Hayakawa K, Kitaura K (2001) Towards ideal NO_x control technology using a plasma-chemical hybrid process. *IEEE Trans Ind Appl* 37(5):1492–1498
12. Conrads H, Schmidt M (2000) Plasma generation and plasma sources. *Plasma Sour Sci Technol* 9(4):441–454
13. Tendero C, Tixier C, Tristant P, Desmason J, Leprince P (2006) Atmospheric pressure plasmas: a review. *Spectrochim Acta Part B Atomic Spectrosc* 61(1):2–30
14. Samukawa S, Hori M, Rauf S, Tachibana K, Kroesen G, Whitehead JC, Murphy AB, Gutsol AF, Starikovskaia S, Kortshagen U, Boeuf J-P, Sommerer TJ, Kushner MJ, Czarnetzki U, Mason N (2012) The 2012 plasma roadmap. *J Phys D Appl Phys* 45(25):253001
15. Whitehead JC (2010) Plasma catalysis: a solution for environmental problems. *Pure Appl Chem* 82(6):1329–1336
16. Chen HL, Lee HM, Chen SH, Chang MB, Yu SJ, Li SN (2009) Removal of volatile organic compounds by single-stage and two-stage plasma catalysis systems: a review of the performance enhancement mechanisms, current status, and suitable applications. *Environ Sci Technol* 43(7):2216–2227
17. Jolibois J, Takashima K, Mizuno A (2012) Application of a non-thermal surface plasma discharge in wet condition for gas exhaust treatment: NO_x removal. *J Electrostat* 70:300–308
18. Yamamoto T, Member S, Yang C-L, Beltran MR, Kravets Z (2000) Plasma-assisted chemical process for NO_x control. *IEEE Trans Ind Appl* 36(3):923–927
19. Miessner H, Francke K-P, Rudolph R (2002) Plasma-enhanced HC-SCR of NO_x in the presence of excess oxygen. *Appl Catal B Environ* 36:53–62
20. McAdams R, Beech P, Shawcross JT (2008) Low temperature plasma assisted catalytic reduction of NO_x in simulated marine diesel exhaust. *Plasma Chem Plasma Process* 28:159–171
21. Tran D, Aardahl C, Rappe K, Park P, Boyer C (2004) Reduction of NO_x by plasma-facilitated catalysis over In-doped γ -alumina. *Appl Catal B Environ* 48:155–164
22. Kim HH, Takashima K, Katsura S, Mizuno A (2001) Low-temperature NO_x reduction processes using combined systems of pulsed corona discharge and catalysts. *J Phys D Appl Phys* 34(4):604
23. Bröer S, Hammer T (2000) Selective catalytic reduction of nitrogen oxides by combining a non-thermal plasma and a V₂O₅-WO₃/TiO₂ catalyst. *Appl Catal B Environ* 28(2):101–111

24. Oda T, Kato T, Takahashi T, Shimizu K (1998) Nitric oxide decomposition in air by using nonthermal plasma processing with additives and catalyst. *IEEE Trans Ind Appl* 34(2):268–272
25. Puchkarev V, Gundersen M (1997) Energy efficient plasma processing of gaseous emission using a short pulse discharge. *Appl Phys Lett* 71(23):3364–3366
26. Gentile AC, Kushner MJ (1995) Reaction chemistry and optimization of plasma remediation of N_xO_y from gas streams. *J Appl Phys* 78(3):2074–2085
27. Oda T (2003) Non-thermal plasma processing for environmental protection: decomposition of dilute VOCs in air. *J Electrostat* 57(3–4):293–311
28. Li J, Ke R, Li W, Hao J (2008) Mechanism of selective catalytic reduction of NO over Ag/Al₂O₃ with the aid of non-thermal plasma. *Catal Today* 139:49–58
29. Nasonova A, Pham HC, Kim D-J, Kim K-S (2010) NO and SO₂ removal in non-thermal plasma reactor packed with glass beads-TiO₂ thin film coated by PCVD process. *Chem Eng J* 156:557–561
30. Oda T, Kato T, Takahashi T, Shimizu K (1997) Nitric oxide decomposition in air by using non-thermal plasma processing-with additives and catalyst. *J Electrostat* 42:151–157
31. Jögi I, Erne K, Haljaste A, Laan M (2013) Oxidation of nitrogen oxide in hybrid plasma-catalytic reactors based on DBD and Fe₂O₃. *Eur Phys J Appl Phys* 61(02):24305
32. Futamura S, Zhang A, Einaga H, Kabashima H (2002) Involvement of catalyst materials in nonthermal plasma chemical processing of hazardous air pollutants. *Catal Today* 72(3):259–265
33. Fan X, Zhu T, Wang M, Li X (2009) Removal of low-concentration benzene in air using a combined plasma catalysis system. *Chemosphere* 75(10):1301–1306
34. Chang C-L, Lin T-S (2005) Elimination of carbon monoxide in the gas streams by dielectric barrier discharge systems with Mn catalyst. *Plasma Chem Plasma Process* 25(4):387–401
35. Jarrige J, Vervisch P (2009) Plasma-enhanced catalysis of propane and isopropyl alcohol at ambient temperature on a MnO₂-based catalyst. *Appl Catal B Environ* 90(1):74–82
36. Van Durme J, Dewulf J, Sysmans W, Leys C, Van Langenhove H (2007) Efficient toluene abatement in indoor air by a plasma catalytic hybrid system. *Appl Catal B Environ* 74(1–2):161–169
37. Subrahmanyam C (2009) Catalytic non-thermal plasma reactor for total oxidation of volatile organic compounds. *Indian J Chem* 48(August):1062–1068
38. Morales MR, Barbero BP, Cadús LE (2008) Evaluation and characterization of Mn–Cu mixed oxide catalysts for ethanol total oxidation: influence of copper content. *Fuel* 87(7):1177–1186
39. Morales MR, Barbero BP, Lopez T, Moreno A, Cadús LE (2009) Evaluation and characterization of Mn–Cu mixed oxide catalysts supported on TiO₂ and ZrO₂ for ethanol total oxidation. *Fuel* 88(11):2122–2129
40. Vitello P, Penetrante B, Bardsley J (1994) Simulation of negative-streamer dynamics in nitrogen. *Phys Rev E* 49(6):5574
41. Pekárek P S, Usama P K (2011) Ozone generation by surface dielectric barrier discharge with TiO₂ photocatalyst. In: 30th ICPIG. pp 10–13
42. Blin-Simiand N, Tardiveau P, Risacher A, Jorand F, Pasquiers S (2005) Removal of 2-heptanone by dielectric barrier discharges—the effect of a catalyst support. *Plasma Process Polym* 2(3):256–262
43. Ogata A, Saito K, Kim H-H, Sugawara M, Aritani H, Einaga H (2010) Performance of an ozone decomposition catalyst in hybrid plasma reactors for volatile organic compound removal. *Plasma Chem Plasma Process* 30(1):33–42